

LOW ORDER MULTIDISCIPLINARY OPTIMISATION OF COUNTER-ROTATING OPEN ROTORS

D. A. Smith - Dale.smith@manchester.ac.uk^{*,†}

A. Filippone - A.Filippone@manchester.ac.uk^{*}

N. Bojdo - nicholas.bojdo@manchester.ac.uk^{*}

^{*}School of MACE, University of Manchester, Manchester, M13 9PL, UK.

[†]Corresponding author

Abstract

A recent renewed interest in CROR propulsion demands the need for suitable design and analysis tools. As an unconventional propulsion system, a multidisciplinary analysis should be made at the preliminary design stage in order to fully evaluate a designs suitability across a number of domains. To address this, this contribution presents a number of low order models ideally suited for the preliminary design stage. Low order models for the evaluation of aerodynamic, acoustic and structural performance are presented. Following this, a multi-objective optimisation is carried out. Suitable objective functions are presented to evaluate the performance over a number of flight phases. Using these, a number of designs are presented for take-off only, cruise only, and combined take-off and cruise. These designs are shown to be of greater performance with respect to a baseline design. The work presented highlights the potential of the low order models and optimisation routine as a preliminary design and analysis tool for CROR propulsion.

NOMENCLATURE

Abbreviations

BPF	Blade Passage Frequency
CROR	Counter Rotating Open Rotor
GA	Genetic Algorithm
SPL	Sound Pressure Level

Roman Symbols

A	Blade element area [m ²]
c	Blade element chord [m]
c_0	Speed of sound [m/s]
c_l, c_d	Sectional lift and drag coefficients [-]
C_a, C_n	Axial and normal force coefficients [-]
$f_D(x), f_L(x)$	Drag and lift chordwise distributions [-]
F_T	Prandtl tip/hub loss factor [-]
g	Axial spacing between rotors [m]
$H(x)$	Thickness chordwise distribution [-]
I_{xx}, I_{yy}	Moments of inertia [m ⁴]

Copyright Statement

The authors confirm that they, and/or their company or organization, hold copyright on all of the original material included in this paper. The authors also confirm that they have obtained permission, from the copyright holder of any third party material included in this paper, to publish it as part of their paper. The authors confirm that they give permission, or have obtained permission from the copyright holder of this paper, for the publication and distribution of this paper as part of the ERF proceedings or as individual offprints from the proceedings and for inclusion in a freely accessible web-based repository.

j	Complex variable, $\sqrt{-1}$ [-]
$J_\nu(Z)$	Bessel function of order ν and argument Z [-]
k_1, k_2	Acoustic and load harmonics [-]
k_x, k_y	Chordwise wave numbers [-]
\dot{m}	Mass flow rate [kg/s]
M_r, M_T	Relative and rotational tip Mach numbers [-]
M_x, M_y	Axial and tangential bending moments [N · m]
N	Rotor blade count [-]
p'	Acoustic pressure [N/m ²]
Q	Rotor torque [N · m]
r_x, r_y, r_z	Observer location distances [m]
r	Blade element radius [m]
R	Blade tip radius [m]
t_c	Thickness-chord ratio [-]
T	Rotor thrust [N]
V	Velocity component [m/s]

Greek Symbols

α	Local angle of attack [rad]
η	Propulsive efficiency [-]
θ	Blade setting/observer angle [rad]
κ	Interference coefficient [-]
ν	Induced velocity component [m/s]
ξ	Objective value [-]
ρ	Density [kg/m ³]
σ	Blade stress [N/m ²]
Ω	Rotor rotational speed [rad/s]
ϕ	Local inflow angle [rad]
ϕ_l, ϕ_s	Lean and sweep phase terms [-]
φ_l	Observer angle [rad]

Ψ_V, Ψ_D, Ψ_L Fourier transforms of thickness, lift and drag distributions [-]

Subscripts

[·]_{1,2} Fore/aft rotor
 [·]_i Self-induced component
 [·]_{mi} Mutually-induced component
 [·]_x Axial component
 [·]_θ Tangential component

1. INTRODUCTION

Aviation now accounts for an increasingly significant amount of the world's environmental emissions. As a result of the increasing concern for the environment, the European Union has introduced a number of emission targets in an attempt to reduce the impact of the aviation industry. For example, by 2020 CO₂ emissions should be 43% lower and NO_x, 80% lower^[1]. Due to these demanding targets, there is a renewed interest in the Counter Rotating Open Rotor (CROR) concept, promising significant efficiency gains over advanced single rotation propellers and turbofan technologies. However, challenges surrounding their noise emissions must be addressed before they can be successfully introduced into commercial aviation. This is exemplified by a further EU target of a 50% reduction in aircraft perceived noise by 2020^[2].

When considering a new concept, there must be sufficient design and analysis tools at the preliminary design stage to ensure time isn't wasted in the later stages of the design with unsuitable concepts. Despite the increasing availability of high-performance computing, the run times and memory required for high order models remains too great for the preliminary design stage. This is due to the fact that at the preliminary design stage, a large design space is considered, and hence a large number of geometry combinations must be analysed. As a result of this, there remains a need for low order designs tools, particularly during the early stages of design.

To address this, this contribution presents a number of low order models for the analysis of a CROR blade pair. Models are developed to evaluate the aerodynamic, aeroacoustic and structural performance of a given CROR design and operating point. These models have been developed to capture as much of the physics of CROR performance whilst minimising the computational cost. Due to their low computational cost, these models are well suited for preliminary design. As such, this paper also presents a multi-objective optimisation routine for use as a design tool.

This work begins by presenting the low order

models developed for CRORs. Firstly, a Blade Element Momentum Theory (BEMT) model is presented for the aerodynamic analysis, after which the acoustic model is presented. Following this, a beam bending method is presented to calculate blade root stress. Upon presentation of the low order models, a Genetic Algorithm (GA) optimisation routine is discussed, as well as the design of suitable objective functions to evaluate a design's global performance. Objective functions for single and dual operating points are discussed. The low order models and the GA are then used to perform a preliminary design of a CROR blade pair. Designs that optimise cruise only, take-off only and combined take-off and cruise are presented. Finally, conclusions from the work are discussed.

2. AERODYNAMIC MODEL

2.1 Momentum Theory

Momentum theory for the isolated rotor is insufficient to describe the behaviour of the dual rotation rotor. Applying the isolated momentum theory to both rotors does not capture the significant interactions that occur both upstream and downstream between the two rotors. To this end, the isolated theory has been extended to the case of dual rotating rotors, particularly, CRORs.

To extend the isolated theory to the dual rotation case, we introduce a set of mutually induced velocities. These mutually induced velocities represent the interaction between both rotors and simply update the apparent velocity seen by each rotor.

We start the extension to the dual rotating case by considering an updated schematic of the rotor flowfield, this is shown in Figure 1. From the

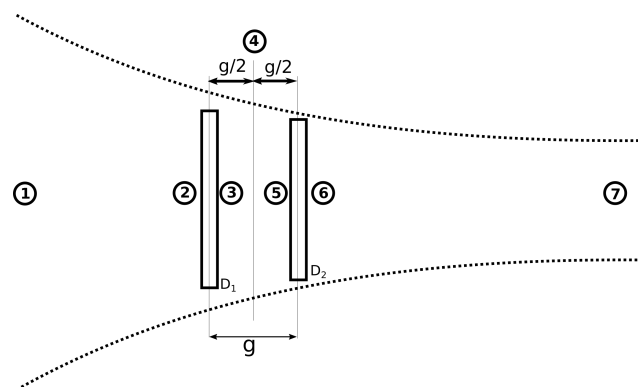


Figure 1: Momentum theory schematic

schematic, we see the bounding streamtube surrounds both rotors. There is a pressure jump over each rotor which are separated by an axial distance,

g. The domain is compromised of a number of discrete zones, where reference is made to a self and mutually induced velocity component. The velocity at each of these zones is summarised in Table 1.

Table 1: CROR velocity components.

Component	Axial	Tangential
V_1	V_∞	0
V_2	$V_1 + \nu_{mi_{x_1}}$	$\nu_{mi_{\theta_1}}$
V_3	$V_2 + \nu_{i_{x_1}}$	$\nu_{i_{\theta_1}} + \nu_{mi_{\theta_1}}$
V_4	$V_3 + \kappa_{D_1} \nu_{i_{x_1}}$	$V_3 + \kappa_{D_1} \nu_{i_{\theta_1}}$
V_5	$V_3 + \nu_{mi_{x_2}}$	$V_3 + \nu_{mi_{\theta_2}}$
V_6	$V_5 + \nu_{i_{x_2}}$	$V_5 + \nu_{i_{\theta_2}}$
V_7	$V_5 + \kappa_{D_2} \nu_{i_{x_2}}$	$V_5 + \kappa_{D_2} \nu_{i_{\theta_2}}$

As discussed, these mutually induced components describe the interaction between the rotors and represent an apparent velocity seen by each rotor due to the opposing rotor. Therefore, the mutually induced components are the product of the self induced component of the opposite rotor, and an 'interference coefficient', i.e.:

$$(1) \begin{aligned} \nu_{mi_{x_1}} &= \kappa_{x_{21}} \nu_{i_{x_2}}; \\ \nu_{mi_{x_2}} &= \kappa_{x_{12}} \nu_{i_{x_1}}; \\ \nu_{mi_{\theta_1}} &= \kappa_{\theta_{21}} \nu_{i_{\theta_2}}; \\ \nu_{mi_{\theta_2}} &= \kappa_{\theta_{12}} \nu_{i_{\theta_1}}. \end{aligned}$$

Where, e.g. $\nu_{mi_{x_1}}$ characterises the effect of the axial velocity of the aft rotor acting on the fore rotor, with analogous definitions for the remaining terms.

The interference coefficients represent the propagation of the self induced components in the direction towards the opposing rotor. From physical reasoning and results from classical momentum theory, Beaumier^[3] gives the following description and values of these interference coefficients:

- $\kappa_{x_{12}} \in [1 : 2]$; the induced velocity far downstream is twice that at the rotor disc;
- $\kappa_{x_{21}} \in [0 : 1]$; the induced velocity is zero far upstream of the disc and equal to one at the disc;
- $\kappa_{\theta_{12}} \approx 2$; the induced swirl quickly approaches 2 behind the rotor;
- $\kappa_{\theta_{21}} \approx 0$; the swirl from the aft rotor does not propagate upstream.

From these descriptions, and in an attempt to account for the effects of axial spacing between the

two rotors, the following expressions have been developed for the interference coefficients:

$$(2) \begin{aligned} \kappa_{x_{12}} &= \left(\frac{g}{2R} + 1 \right), \\ \kappa_{x_{21}} &= \left(1 - \frac{g}{2R} \right), \\ \kappa_{\theta_{12}} &= \left(\left(\frac{g}{2R} \right)^{1/4} + 1 \right), \\ \kappa_{\theta_{21}} &= 0. \end{aligned}$$

Also note that the additional interference terms κ_{D_1} and κ_{D_2} used to calculate the mutually induced terms other than at the rotor plane are simply related to the original terms, as such:

$$(3) \begin{aligned} \kappa_{D_1} &= \kappa_{x_{21}} \left(g = \frac{g}{2} \right), \\ \kappa_{D_2} &= \kappa_{x_{12}} (g = 4R). \end{aligned}$$

With a greater understanding of the flow, we now proceed with the development of the new momentum theory equations for the dual rotor case. The total thrust produced by the CROR is given by the increase in momentum through the streamtube, this total thrust must be equal to the sum of thrust from each rotor, i.e.:

$$(4) T = T_1 + T_2.$$

The individual thrust from each rotor is then examined. For the fore rotor, this is taken as the change in momentum far upstream and the midpoint between the two rotors, i.e.:

$$(5) T_1 = \dot{m}_1 (V_4 - V_1),$$

The aft rotor thrust is computed from the change in momentum between this midpoint and far downstream, i.e.:

$$(6) T_2 = \dot{m}_2 (V_7 - V_4).$$

For small axial spacings, the mass flow for each rotor is comparable. With this, summing Equations (5) and (6), we arrive at our original expression for the total thrust.

Now expanding the velocity terms in Equation (5), the fore thrust is given by:

$$(7) T_1 = \dot{m}_1 (V_1 + \nu_{mi_{x_1}} + \kappa_{D_1} \nu_{i_{x_1}} - V_1).$$

With the mass flow through the fore rotor given by,

$$(8) \dot{m}_1 = \rho A_1 (V_1 + \nu_{i_{x_1}} + \nu_{mi_{x_1}}),$$

Expanding the velocity terms further, the thrust produced by the fore rotor becomes:

$$(9) \quad T_1 = \rho A_1 (V_1 + \nu_{ix_1} + \kappa_{x_{21}} \nu_{ix_2}) (\kappa_{x_{21}} \nu_{ix_2} + \kappa_{D_1} \nu_{ix_1}).$$

Now consider the aft rotor, expanding the velocity terms in Equation 6, the thrust produced by the aft rotor is:

$$(10) \quad T_2 = \dot{m}_2 (V_1 + \nu_{mix_1} + \nu_{mix_2} + \kappa_{D_2} \nu_{ix_2} - (V_1 + \nu_{mix_1} + \kappa_{D_1} \nu_{ix_1})),$$

with the mass flow through the aft rotor given by,

$$(11) \quad \dot{m}_2 = \rho A_2 (V_1 + \nu_{ix_1} (1 + \kappa_{x_{12}}) + \nu_{ix_2} (1 + \kappa_{x_{21}})),$$

and again further expanding velocity terms, the thrust produced by the aft rotor is thus:

$$(12) \quad T_2 = \rho A_2 (V_1 + \nu_{ix_1} (1 + \kappa_{x_{12}}) + \nu_{ix_2} (1 + \kappa_{x_{21}})) (\nu_{ix_1} (\kappa_{x_{12}} - \kappa_{D_1}) + \kappa_{D_2} \nu_{ix_2}).$$

Now considering the torque produced by the CROR blade pair. The torque is given as the change in angular momentum through the streamtube. Note, as the rotors rotate in opposite directions, the total torque is computed as the difference between the torque of the two rotors. Considering the fore rotor:

$$(13) \quad \begin{aligned} Q_1 &= V_{t_1} r_1 \dot{m}_1, \\ &= \rho r_1 A_1 (\nu_{i\theta_1} - \kappa_{i\theta_{21}} \nu_{i\theta_2}) \\ &\quad (V_1 + \nu_{ix_1} + \kappa_{x_{21}} \nu_{ix_2}). \end{aligned}$$

The torque produced by the aft rotor is calculated in a similar fashion,

$$(14) \quad \begin{aligned} Q_2 &= V_{t_3} r_2 \dot{m}_2, \\ &= \rho r_2 A_2 (\nu_{i\theta_2} - \kappa_{i\theta_{12}} \nu_{i\theta_1}) \\ &\quad (V + \nu_{ix_1} (1 + \kappa_{x_{12}}) + \nu_{ix_2} (1 + \kappa_{x_{21}})). \end{aligned}$$

These equations are then considered in elemental form, i.e. dT and dQ , by considering the elemental area, $dA = 2\pi r dr$. From this, constant loading is not assumed over the blade span and the induced velocities are free to take their own form.

Hence we now have a set of equation to compute the elemental thrust and torque of a CROR, formulated from momentum theory that accounts for the interaction between the two rotors.

2.2 Blade Element Theory

The extension of Blade Element Theory (BET) from the isolated case to the dual rotor case requires the velocity triangles to be updated with the mutually induced components and then the thrust

and torque re-evaluated. This then allows for the interaction between the two rotors to be accounted for with BET. The relative velocity at a given blade element is then:

$$(15) \quad \begin{aligned} V_{rel} &= \sqrt{V_x^2 + V_\theta^2}, \\ &= \sqrt{(V_\infty + \nu_{ix} + \nu_{mix}) + (\Omega r - \nu_{i\theta} + \nu_{mi\theta})}. \end{aligned}$$

This equation is applied to both rotors, using the appropriate induced velocity terms for each rotor. The thrust produced by each blade element is then,

$$(16) \quad dT = \frac{1}{2} F_T N \rho V_{rel}^2 C_a c dr,$$

and the torque,

$$(17) \quad dQ = \frac{1}{2} F_T N \rho V_{rel}^2 C_n c r dr.$$

F_T is the Prandtl correction factor^[4,5], and C_a and C_n are the axial and normal force coefficients:

$$(18) \quad \begin{bmatrix} C_a \\ C_n \end{bmatrix} = \begin{bmatrix} \cos \phi & -\sin \phi \\ \sin \phi & \cos \phi \end{bmatrix} \begin{bmatrix} c_l \\ c_d \end{bmatrix},$$

c_l , and c_d are the sectional lift and drag coefficients, taken from a look up table for the sectional angle of attack,

$$(19) \quad \alpha = \theta - \phi,$$

where, θ is the local blade setting angle, and ϕ , the local inflow angle. With the updated velocity triangles this is then,

$$(20) \quad \phi = \tan^{-1} \left(\frac{V_\infty + \nu_{ix} + \nu_{mix}}{\Omega r - \nu_{i\theta} + \nu_{mi\theta}} \right).$$

Hence, with the simple addition of the mutually induced velocities to the isolated velocity triangles, the BET has been extended for the dual rotor case, in particular for CRORs.

2.3 Combined BEMT

In order to provide a robust and reliable solution methodology, the blade element and momentum theories are combined. First, an initial guess is made of the induced velocities, $\nu_i^{(0)}$. The thrust and torque are then computed using the BET equations, Equations (16) and (17). The blade element and momentum equations are then combined, e.g.:

$$(21) \quad dT_1|_{BET} - dT_1|_{MT}(\nu_{ix_1}, \nu_{ix_2}, \nu_{i\theta_1}, \nu_{i\theta_2}) = 0,$$

resulting in a system of non-linear equations. To solve, a Newton-step method is used to solve an

inner iteration of the induced velocity. An outer iteration using an under-relaxed successive substitution scheme^[6] is then used to compute the thrust and torque using blade element theory. The iteration loop is then exited when the error between successive computations has met a given tolerance. The final blade element theory computation is used as the final values for thrust and torque.

2.4 Model Validation

A number of previous experimental studies were used to validate the aerodynamic model. For the sake of brevity, a comparison with only a single study is presented here, comparing thrust coefficient and flowfield velocities. The thrust coefficient was computed for a 0.409 [m] diameter, 4x4 CROR. The rotor blades were of SR2 design. The SR2 spanwise geometry is shown in Figure 2. Figure 3 shows

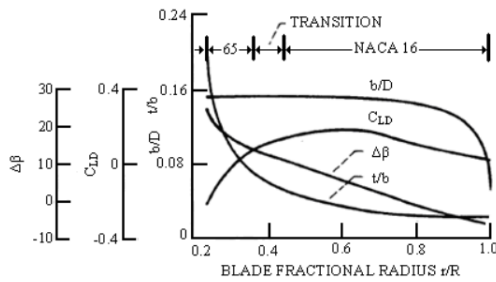


Figure 2: SR2 spanwise geometry^[7]

the comparison between the thrust coefficient computed using BEMT and the experimental data obtained by Dunham *et al.*^[8]. This for a fore and aft blade setting angle of $\theta_{.75} = 41.34$ [°] over a number of advance ratios. From the comparison

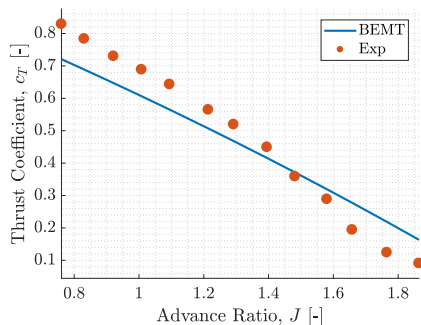


Figure 3: SR2 thrust coefficient comparison.

with the experimental data, it can be seen that the BEMT model computes the thrust coefficient relatively well over all advanced ratios. The largest discrepancies occur at the lowest and highest advance ratios where blade angles are at their two extremes. This then a result of the sectional aerodynamics.

Flow field data, specifically axial and tangential velocities are then compared against the same propeller at the same pitch angle at an advance ratio of $J = 1.21$ [-]. These comparisons are shown in Figures 4 and 5, where values obtained using BEMT and those obtained by Dunham *et al.*^[8] using PIV in a plane at $\frac{g}{D} = 0.15$ downstream of the aft rotor are compared.

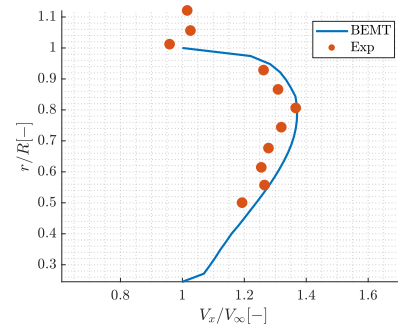


Figure 4: SR2 axial velocity downstream of aft rotor.

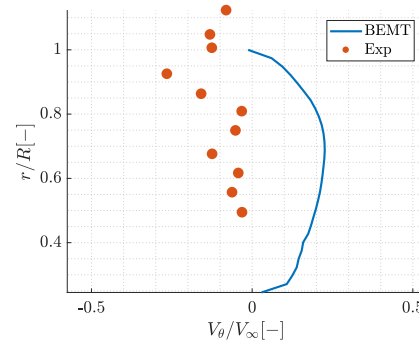


Figure 5: SR2 tangential velocity downstream of aft rotor.

It can be seen that the axial velocity is predicted quite well, and this was found to be the case along a number of axial locations. On the other hand, the tangential velocity is not computed as well, and this was again found to be the case when compared at a number of axial planes. The experimental results show the tangential velocity between the fore and aft rotors is almost completely cancelled behind the aft rotor, and this is not captured by the BEMT model.

With the comparisons of the BEMT model against experimental data, it can be seen in general that the data compares sufficiently well. This gives confidence in the model to perform preliminary investigations on the performance of CRORs, as well as within a preliminary design tool.

3. AEROACOUSTIC MODEL

The noise emission forms an important aspect of the environmental impact of modern aircraft. Therefore, the study of the noise is a critical part of the propulsor design. The tonal noise of CRORs can be considered in two parts, rotor alone tones and interaction tones. Rotor alone tones can be calculated using isolated rotor noise theory. The interaction tones are further divided into two additional components, acoustic interaction and aerodynamic interaction^[9]. The acoustic interaction is computed by summing the isolated pressure signals calculated for each rotor. Summing the two signals will result in constructive and destructive addition of the signals, hence the acoustic interaction. The aerodynamic interaction occurs due to the unsteady loading that results from the interaction of the potential fields propagating up and downstream, as well as the wake interaction on the aft rotor. In this work, only the unsteady loading on the aft rotor due to wake interaction is considered. It is hoped to add the potential field interactions as part of the future work.

3.1 Steady Noise

We start by considering the rotor alone tones. For this we consider the tonal noise of the isolated rotor. The tonal noise is composed of contributions from thickness and loading sources. From Hanson^[10] the acoustic pressure due to the rotating rotor is given by:

$$(22) \quad p'(x, t) = \frac{-\rho c_0^2 N \sin \theta}{4\pi(r_z/R)(1 - M_\infty \cos \theta)} \sum_{k_1=-\infty}^{\infty} \exp \left\{ j \left(k_1 N \Omega_D \left(\frac{r_l}{c_0} - t \right) + k_1 N \left(\varphi_l - \frac{\pi}{2} \right) \right) \right\} \times \int_0^1 M_r^2 e^{j(\phi_l + \phi_s)} J_{(Nk_1)} \left(\frac{k_1 N \bar{r} M_T \sin \theta}{1 - M_x \cos \theta} \right) \begin{Bmatrix} \mathcal{V} \\ D \\ L \end{Bmatrix} d\bar{r},$$

k_1 is the acoustic harmonic, and the observer locations r_z , r_l , and θ_l are as defined in Figure 6. ϕ_l and

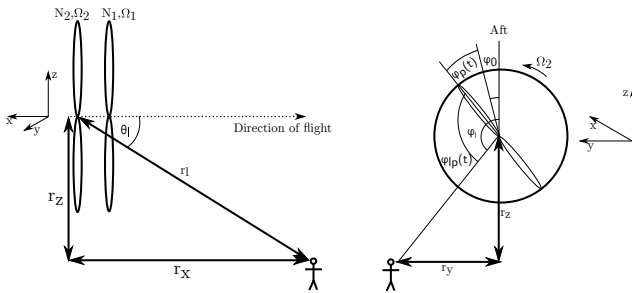


Figure 6: Observer location definitions.

ϕ_s are phase terms due to blade lean and sweep.

$J_\nu(Z)$ is a Bessel function of the first kind, of order ν and argument Z . M_T is the tip Mach number and M_r , the relative Mach number at each radial element. The term $1 - M_x \cos \theta$, is the Doppler frequency shift, with θ the retarded observer angle. \mathcal{V} , D , and L , are the sources terms due to thickness and drag and lift forces respectively. These are given by:

$$(23) \quad \begin{Bmatrix} \mathcal{V} \\ D \\ L \end{Bmatrix} = \begin{Bmatrix} k_x^2 t_c \Psi_V \\ j k_x \frac{c_d}{2} \Psi_D \\ j k_y \frac{c_l}{2} \Psi_L \end{Bmatrix}.$$

With t_c , c_l , and c_d the thickness-chord ratio, and lift and drag coefficients respectively. The chordwise wave numbers, k_x and k_y , which represent non-compactness factors are given by:

$$(24) \quad k_x = \frac{k_1 N c M_T}{R M_r (1 - M_x \cos \theta)},$$

$$k_y = \frac{k_1 N c}{M_r r} \left(\frac{M_r^2 \cos \theta - M_x}{1 - M_x \cos \theta} \right).$$

Finally, the terms Ψ_V , Ψ_L , and Ψ_D are the Fourier transforms of the thickness, lift and drag chordwise distributions. These are given by^[11]:

$$(25) \quad \begin{Bmatrix} \Psi_V \\ \Psi_D \\ \Psi_L \end{Bmatrix} = \int_{-\frac{1}{2}}^{\frac{1}{2}} \begin{Bmatrix} H(x) \\ f_D(x) \\ f_L(x) \end{Bmatrix} \exp(j k_x x) dx.$$

Where, $H(x)$, $f_D(x)$, and $f_L(x)$, describe the thickness and loading distributions along the blade section chord.

3.2 Unsteady Loading Noise

The aerodynamic interaction noise results from the aft rotor cutting through the wake of the fore rotor. This leads to an unsteady loading on the aft rotor, which occurs at harmonics of the fore rotor BPF. The acoustic pressure of an unsteadily loaded rotor at a load harmonic k_1 is given by Hanson^[9] as:

$$(26) \quad p_2'(x, t) = \frac{-\rho c_0^2 N_2 \sin \theta}{4\pi(r_z/R_2)(1 - M_x \cos \theta)} \sum_{k_1=-\infty}^{+\infty} \sum_{k_2=-\infty}^{+\infty} \exp \left\{ j \left[(k_1 N_2 \Omega_2 + k_2 N_1 \Omega_1) \left(\frac{r_l}{c_0} - t \right) + (k_1 N_2 - k_2 N_1) \left(\varphi_l - \frac{\pi}{2} \right) \right] \right\} \times \int_{\bar{r}_{h_2}}^{\bar{r}_{t_2}} M_r^2 e^{j(\phi_s + \phi_l)} J_{k_1 N_2 - k_2 N_1} \left[\frac{(k_1 N_2 + k_2 N_1 \Omega_{12}) \bar{r}_2 M_{T_2} \sin \theta}{1 - M_x \cos \theta} \right] \times \left\{ j k_y \frac{C_{l_2}^{(k_1)}}{2} \Psi_{L_2}^{(k_1)} + j k_{x_2} \frac{C_{d_2}^{(k_1)}}{2} \Psi_{D_2}^{(k_1)} \right\} d\bar{r}_2.$$

Again, the observer location definitions are given in Figure 6, note the reference to the aft rotor. Here, the non-dimensional wave numbers (again characterising non-compactness) are given by:

$$(27) \quad k_{x_2} = \frac{c_2 M_{T_2}}{R_2 M_{r_2}} \left[\frac{k_1 N_2 + k_2 N_1 \Omega_{12}}{1 - M_x \cos \theta} - k_2 N_1 (1 + \Omega_{12}) \right],$$

$$(28) \quad k_{y_2} = -\frac{c_2 M_{T_2}}{R_2 M_{r_2}} \left[\frac{(k_1 N_2 + k_2 N_1 \Omega_{12}) M_{r_2}^2 \bar{r}_2 \cos \theta}{1 - M_x \cos \theta} - \frac{M_\infty (k_1 N_2 - k_2 N_1)}{\bar{r}_2} \right].$$

The terms in the above equations are as those for the isolated rotor case, and $\Omega_{12} = \frac{\Omega_1}{\Omega_2}$. Note that as the thickness noise is unaffected by the unsteady loading, it should therefore be calculated using Equation (22). In the above equation, k_1 is the acoustic harmonic, whilst k_2 is the load harmonic.

This equation can be applied to any general case of a rotor under any unsteady loading i.e. it may be applied to calculate the unsteady loading noise of the fore rotor due to potential interactions from the aft rotor. Parry^[12] presents a thorough development for unsteady loading applied to CRORs. Specifically, the equations for the unsteady loading due to interaction of the aft rotor with the fore wake presented by Parry were employed within this work.

Thus we have a number of equations that can be used to describe the acoustic emissions of a CROR blade pair, accounting for both acoustic and aerodynamic interactions between rotors.

3.3 Model Validation

Similarly to the aerodynamic model, a number of test cases were used to validate the CROR acoustic model. Again for the sake of brevity only a single case will be presented to demonstrate the model performance.

The acoustic pressure of the 4x4 SR2 CROR was computed in experiments by Block^[13]. Here, data was taken for an array of microphones at various axial locations, with the rotors at a setting angle of $\theta_{.75} = 13.3$ [°] rotating at 10,000 [rev/min]. Figure 7 presents the comparison between the experimentally obtained SPL and those calculated using the described numerical model for a single microphone location for the first eight harmonics.

From Figure 7, it can be seen that the model predicts the Sound Pressure Level (SPL) relatively well over a number of harmonics when compared with the 'exp method 2' data. The report presented three different signal post-processing methods. It

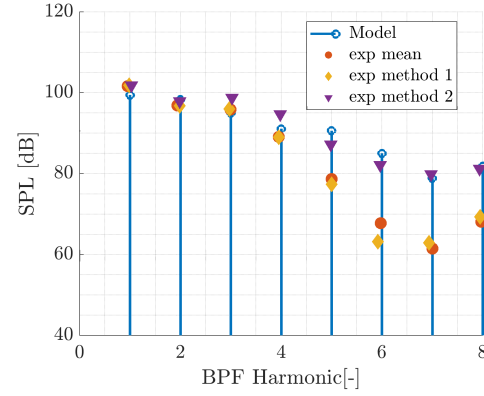


Figure 7: CROR SPL for microphone positions $(x, y, z) = (-0.79, -1, -0.409)$

was reported that the mean and method 1 showed background noise level at higher harmonics with method 2 showing more accurately the rotor noise levels. This agreement between the numerical and *method 2* was seen to be the case for all microphone locations compared. Hence, from the results presented, it can be concluded that the acoustic model can be used with confidence in the investigation of CROR noise and as a tool within a preliminary design routine.

4. Structural Modelling

Rotor blades typically operate at very high rotational rates, and in the case of take-off, operate at very high loading. As a result of this, in the design of any rotor system it is vitally important to determine if a given design has the structural integrity to operate over all flight phases. In this section, a simple model for determining the maximum stress at the blade root is presented.

4.1 Beam Bending Theory

The root stress was computed using beam bending theory. This allowed for rapid estimation of the blades structural integrity. The total stress at the blade root comprises of aerodynamic loading, resulting in bending moments, and a pure tensile stress due to the centrifugal force. In addition to this, if the blade is swept or has lean, the centrifugal forces will give rise to additional bending moments.

4.1.1 Bending Moments due to Blade Loading

With the blade loading, dT and dQ , computed using the aerodynamic model, the resulting bending

moments from beam bending theory are^[14]:

$$(29) \quad M_T = \int_{r_h}^R (r - r_i) \frac{dT}{dr} dr;$$

$$(30) \quad M_Q = \int_{r_h}^R \frac{(r - r_i)}{r_i} \frac{dQ}{dr} dr.$$

With the blades at a given pitch angle, θ , these moments are then resolved into their axial and normal components:

$$(31) \quad \begin{bmatrix} M_x \\ M_y \end{bmatrix} = \begin{bmatrix} \cos \theta & \sin \theta \\ \sin \theta & -\cos \theta \end{bmatrix} \begin{bmatrix} M_T \\ M_Q \end{bmatrix}.$$

Figure 8 shows these resulting moments for a given radial element. The rotor thrust and torque will also

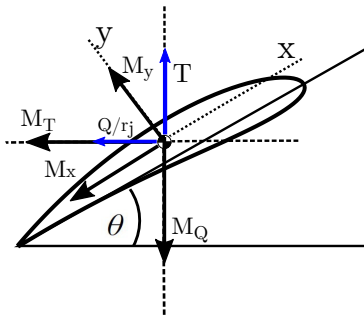


Figure 8: Moment resultant on radial element.

produce a shear stress throughout the blade section. However, this is typically negligible in comparison to the bending moments^[15]. Therefore, the shear due to thrust and torque is not considered in this work.

4.1.2 Blade Centrifugal Force

Centrifugal forces arise due to the rotation of the blade. This centrifugal force resolves into a pure tensile stress. The centrifugal force acting on each radial blade element is given by:

$$(32) \quad dF_c = \Omega^2 r dm,$$

where Ω is the rotor rotational speed in rad/s , and dm is the elemental mass, and assuming a continuous material, is given by:

$$(33) \quad dm = \rho_b A dr.$$

ρ_b is the blade material density, A is the elemental aerofoil area, and dr , the elemental radius. The total centrifugal force resulting from blade rotation is then:

$$(34) \quad F_c = \rho_b \Omega^2 \int_{r_h}^R A r dr.$$

Which yields the centrifugal tensile stress (here, about the blade root):

$$(35) \quad \sigma_c = \frac{F_c}{A_r}.$$

4.1.3 Bending Moments due Centrifugal Force

Bending moments due to centrifugal forces arise if the blade has sweep or lean, or if the mass distribution of the blade is not constant along the blade span. Those moments due to non-continuous mass distribution are typically small in comparison to the other bending moments^[16], as such, they are not considered in this work. The bending moments due to sweep and lean act in the same sense as the thrust and torque bending moments and are thus given by:

$$(36) \quad M_{c_\Lambda} = \sum_i^n dF_{c_i} l_{\Lambda_i}, \quad M_{c_\epsilon} = \sum_i^n dF_{c_i} l_{\epsilon_i},$$

l_Λ and l_ϵ are the sweep and lean bending moment arms. These moments are then transformed to the axial and normal directions and added to the bending moments due to blade loading to give the total moments.

4.1.4 Total Blade Stress

Having computed the bending moments and centrifugal force, the total stress at the blade root is computed as follows:

$$(37) \quad \sigma(x, y) = -\frac{M_x y}{I_{xx}} - \frac{M_y x}{I_{yy}} + \sigma_c.$$

It can be seen that the maximum stress will occur for the maximum distances x and y . Whilst the model here is used to compute the maximum stress at the blade root, it can easily be extended to compute the stress throughout the blade.

Unfortunately, at the time of writing the authors were unable to find suitable data for the validation of the model. Nonetheless, with sufficient care, the model may still be used. This is justified as the computed stress is to be minimised, and specific values are not so significant for this work.

5. OPTIMISATION

In the development of a preliminary design tool, optimisation has been used to find a number of CROR geometries that maximise a number of performance measures and meet given design requirements over a number of operating points.

5.1 Genetic Algorithm

Due to its robustness and its ability to handle complex multi-variable problems, a GA optimisation routine was employed^[17], and extended to evaluate multiple objectives and operating points. The GA is a form of evolutionary algorithm that mimics the behaviour of natural selection. An initial population of Chromosomes, a data set containing the free design parameters (known as Phenotypes), are generated. Their performance with respect to the optimisation goals is then evaluated. Upon evaluation, using processes borrowed from evolution (crossover, mutation, re-insertion), chromosomes are mated to produce a new generation of offspring, with the fittest, or highest performing individuals making it through successive generations or being selected for mating, whilst the poorest performing members die off (survival of the fittest). This process is repeated until termination criteria is met^[18].

In this work, the preliminary design stage is considered. As such, there is a large number of free or design variables for relatively few design constraints. Here, the design constraints are used to represent the operating point of the CROR. Specifically, these were, an operating altitude and Mach number. In addition to these, a power requirement representing the operating point was placed within the objective function.

The free variables within the optimisation represented both rotors rotational speed, as well as the rotor geometry. The geometry included both fore and aft blade counts, their radii, and the axial spacing between them. The sectional aerodynamics were obtained from look up tables for the SC1095 aerofoil^[19]. Of course, this limits the design to just this aerofoil series. However, this allows for the optimisation of chord and twist, without the additional computational expense of computing sectional aerodynamics on the fly. In order to reduce the number of free variables, spanwise varying geometry was parametrised using Bernstein polynomials, a method as described by Kulfan^[20].

Of course, for all these free variables, limits had to be placed on their maximum and minimum values. This, for one thing, ensures realistic geometries are produced. This also ensures geometries are analysed within the limits of the models. For example, the rotor radius and rotational speed are limited in order to avoid high tip Mach numbers. The limits for the non-spanwise varying geometry is summarised in Table 2. Twist was limited to avoid high incidence on the blade element, and the chord was limited relative to the blade radius. Of course, these limits are easily changed for changes in design point, and the values presented here serve to

Table 2: Design variable limits.

Parameter	Minimum	Maximum
Ω_1, Ω_2 [rev/min]	750	1500
R_1, R_2 [m]	0.75	1.50
N_1, N_2 [-]	3	10
$\frac{g}{D_1}$ [-]	0.05	1.00
Clipping [%]	0.00	0.15

give context to the applicability of the design tool.

Within the framework of this work, the objective function is used to describe the performance of a given CROR design. The objective function takes as inputs the free design variables. The aerodynamic, acoustic and structural performance are then computed using the models described within this work. These performance parameters must then be suitably normalised, and a weighting applied in order to give a global performance measure of the given design.

5.2 Single Point Objective Function

We consider first the simple case for a design of a single operating point. For example, a design that is to optimise cruise performance only. Here we describe a suitable objective function that will allow for the global performance of a given design to be evaluated. First, the geometry is generated from the parameterised variables. This, in addition to the operating conditions, are passed to the aerodynamic model. From this, the total shaft power is evaluated and normalised to give the first objective value,

$$(38) \quad \xi_1 = \left| \frac{P_{calc}}{P_{req}} - 1 \right|.$$

From the aerodynamic data, the propulsive efficiency is then computed and normalised to give the second objective value:

$$(39) \quad \xi_2 = 1 - \eta.$$

Note, this normalisation ensures that the efficiency is maximised (as optimisation is a minimisation problem).

Following this, the acoustic model is used to evaluate the SPL produced by the given design. In this work, the observer location was arbitrary, as specific values at this stage are not required, only that the noise should be minimised. Although this can easily be altered to locations of interest, e.g. certification locations. The calculated SPL is then nor-

malised to give the third objective value:

$$(40) \xi_3 = \frac{SPL}{150}.$$

The normalisation value of 150 was chosen as this was found to give suitable normalisation in line with the other performance measures. Note this should be changed for different operating points and observer locations. This is important to avoid any undesirable weighting to this objective value.

The structural performance is then evaluated using the structural model described previously. This is then normalised with respect to the material yield stress,

$$(41) \xi_4 = \frac{\sigma_1}{\sigma_y}, \quad \xi_5 = \frac{\sigma_2}{\sigma_y}.$$

In this work, CFRP composite was used with a yield stress of 1.05 [GPa]. This was used to represent modern materials in rotor blade construction.

Finally, the total objective value must be computed. In this work, the weighted sum approach was taken. An equal weighting can be applied to ensure that the optimiser drives to simultaneously improve each objective. However, other weightings can be applied based on the engineer's judgement. A random weighting can also be considered^[21], this removes further user input and can increase the potential search space. The workflow for the single point objective function is summarised in Figure 9.

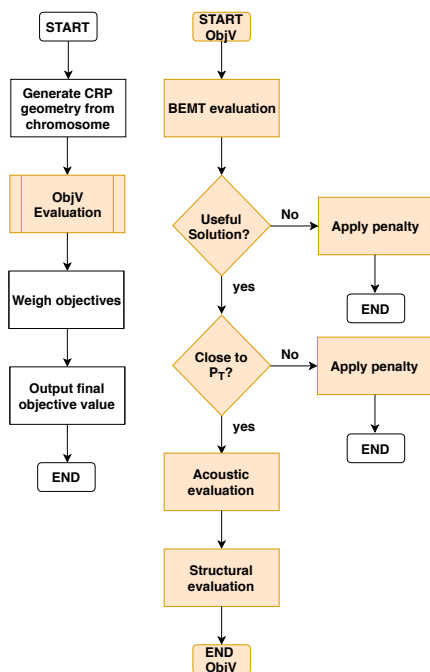


Figure 9: Single point objective function workflow.

5.3 Dual Point Objective Function

We now consider the more complex case of a design for two operating points. To illustrate, we use for example simultaneous optimisation for the cruise and take off conditions. This may represent a realistic scenario, where one may wish to design a CROR to minimise community noise at take-off and maximise propulsive efficiency at cruise. This, therefore, requires that both cruise and take-off performance must be evaluated for each design within the objective function. For this, re-pitching of the rotor blades and/or changes to the rotational speed must be made to change from one operating point to the other. For this work, we consider only pitch changes. In this work, as take-off presents the greatest demands on the rotor, it is first evaluated before re-pitching to the cruise condition for its evaluation.

Starting as for the single point objective function, the geometry and operating point are taken as inputs. The take-off aerodynamic, acoustic and structural performance are then evaluated and their corresponding objective values calculated. The first objective value calculates the proximity of the design to achieving the required power target. It is noted here, that penalties should be applied to designs that are far from the required power, and the objective function evaluation exited at this point. Doing this ensures that designs that cannot achieve take-off power are not considered and the unnecessary cruise computations can then be avoided. Therefore, the optimisation will be observed to perform quickly at the beginning of the optimisation where designs are not computed for cruise as they fail to meet take-off requirements. The optimisation then slows down as the number of individuals that meet take-off requirement increases (and hence the cruise computation is then required). It is noted the penalty should not be so strictly applied to avoid narrowing the design space.

For individuals that meet the given power requirements, the re-pitch calculation is then required to evaluate cruise performance. The re-pitch calculation is first performed using BET. The result from this is then used as the initial guess for the BEMT computation. This was found to significantly reduce the iteration count for the BEMT re-pitch computation. With the new blade setting angle computed the aerodynamic, acoustic and structural objective values can be computed. The overall design objective value is then computed using a weighted sum to provide an objective global performance value to the given design. The workflow for this objective function is shown in Figure 10.

It will be observed that this new objective function will be considerably more computationally ex-

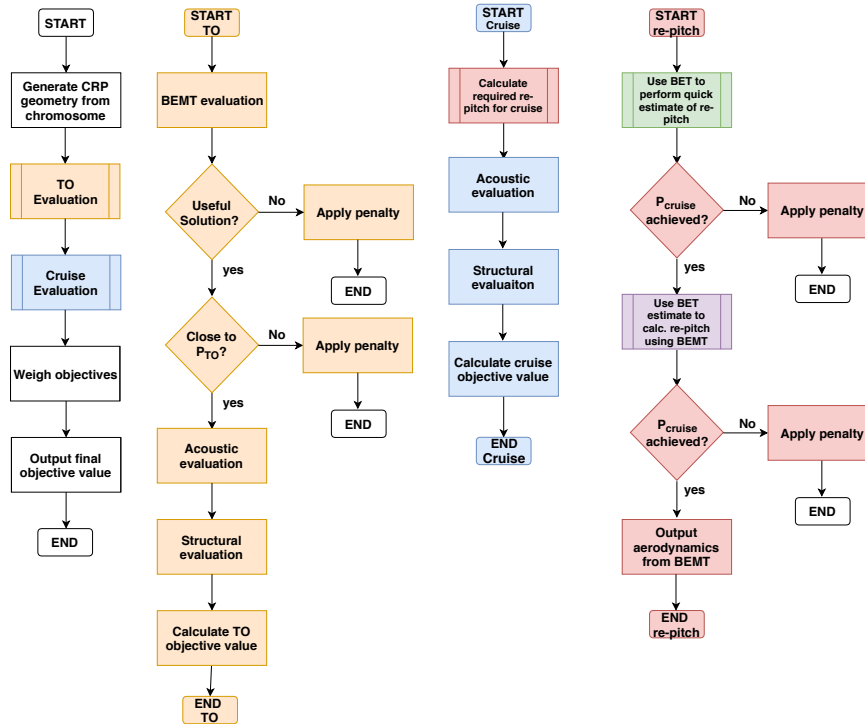


Figure 10: Dual point objective function workflow.

pensive than the single point. This is due to the multiple BEMT evaluations required to calculate the required blade setting angle. This highlights the importance of the low order models to ensure a large design space can be considered in a short time in the preliminary design stage.

The objective function described can be used to evaluate the performance over two CROR operating points. It can easily be extended to analyse additional operating points. However, with increasing number of objectives, the optimisation becomes increasingly more complex. As a result, it may be difficult to find a solution that can suitably perform over all operating points, and greater care must be placed on the weighting of objectives to the requirements of the design.

6. CROR DESIGN

The optimisation routine was used to perform preliminary design for a CROR blade pair for a general aviation class aircraft. Using the single point objective function, designs were computed to maximise cruise only and take-off only performance. Following this, the dual point objective function was used to compute a design to simultaneously maximise cruise and take-off performance. Design objectives were to maximise propulsive efficiency, minimise SPL at an arbitrary observer location and

minimise blade root stress. For this the following weighting was used:

$$(42) \quad \xi = \frac{1}{6} (\xi_1 + 2\xi_2 + 2\xi_3 + 0.5(\xi_4 + \xi_5)) .$$

This gives additional weighting to efficiency and noise performance. This weighting was found to give superior noise and efficiency performance, whilst meeting power requirements and suitable structural integrity maintained when compared to an equal weighting.

Design constraints were used to tailor the design for a general aviation class aircraft. These constraints were the Mach number, altitude and shaft power requirement. The FLIGHT software^[22] was used to compute representative values for cruise and take-off for a general aviation class aircraft. These operating point constraints are summarised in Table 3. Note, the required shaft power is the sum

Table 3: Design operating points

Parameter	Take-off	Cruise
M_∞ [-]	0.2	0.45
Altitude [ft]	0	25,000
P_{req} [kW]	750	450

from both rotors.

After the investigation of various optimisation parameters (e.g. mutation rate, population size, reinsertion rate), designs were carried out for a 250 Chromosome population. Termination of the optimisation was executed when negligible performance gains were observed in successive generations, typically after 150 generations.

To demonstrate the capability of the preliminary design tool, it is best to compare designs against a baseline design. However, with a lack of existing CRORs to compare against, an arbitrary design is developed based on the SR2 design. This baseline consists of 4x3 blades both of which were 3.0 [m] in diameter, and separated by $\frac{g}{D} = 0.15$. Both fore and aft rotors rotate at 1000 [rev/min] and are trimmed to meet the power requirements for equal power share.

For these preliminary designs, additional constraints of equal rotational speeds and power shares and an aft blade count of one less than the fore (co-prime), are imposed. However, these can of course easily become free variables.

Resulting design geometries are summarised in Table 4. The designs for each show use of significant

Table 4: Design geometries

Parameter	Take-off	Cruise	TO & Cruise
$N_1 \times N_2$ [-]	4 × 3	6 × 5	6 × 5
Ω [rev/min]	1060	790	790
R_1 [m]	1.06	1.57	1.73
R_2/R_1 [-]	0.980	1	0.95
g/D [-]	13.8	10.7	19.2

spacing between the two rotors, and show very little clipping. This highlights the need for some modelling of the tip vortex region, as the tip vortex impingement can be a significant noise source. It is interesting to note that the take-off design operates a high-speed low diameter design, whilst the cruise operates the opposite, low speed, high diameter. The cruise condition will be limited to its upper rotational speed before blade losses become significant due to the increased flight speed, even with the lower diameter. This is perhaps why the dual-point design has followed a similar design. It can be seen that the take-off design has opted for a lower blade count than the cruise condition. With the dual point following again the cruise design.

The chord and twist distributions for each case is shown in Figures 11 and 12 respectively. The chord distributions for all fore blades show a similar shape and size, with the cruise design showing a higher blade area. Both the take-off and cruise only de-

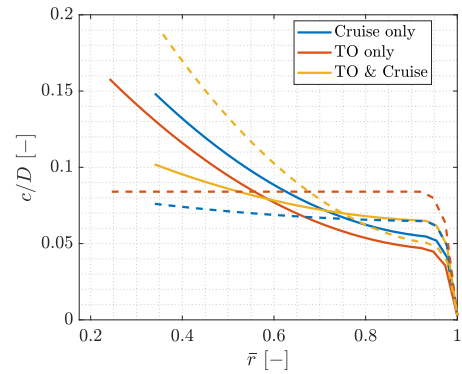


Figure 11: Optimised designs chord distributions. (-) fore, (- -) aft.

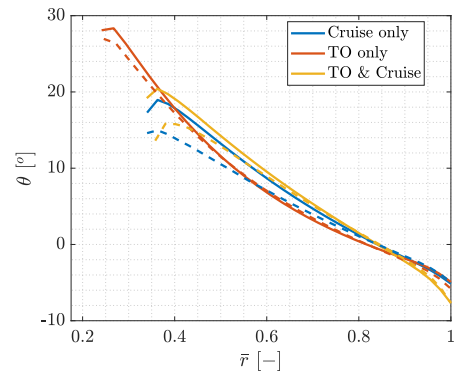


Figure 12: Optimised designs twist distributions. (-) fore, (- -) aft.

signs show almost straight blades for the aft section, this to give a higher blade area to account for the reduced blade count. Similarly for the dual point design, whilst not straight, the blade area is significantly increased compared to the fore. The difference in hub radius is also evident. The hub radius is computed to ensure sufficient space for the blades on the spinner. Therefore, with a higher blade count and root chord the dual point and cruise only designs have a significantly higher hub radii.

Inspecting the twist distributions, it can be seen that all designs have reached a very similar optimum twist distribution. Note in all cases the higher values for the fore compared to the aft. This highlighting the benefits of the mutual interference on the aft rotor.

Table 5 presents the performance of the single point designs relative to the SR2 baseline. Optimal designs were only selected on the basis of meeting power requirements, and for both cases, this was met. It can be seen that both take-off designs offer propulsive efficiency and noise performance gains over the baseline design. However, it can be seen that this comes at the cost of reduction in structural performance. It must be noted though

Table 5: Design Performance (against baseline) for single point.

Parameter	Take-off	Cruise
$\Delta\eta$ [%]	+5.15	+11.9
ΔSPL [dB]	-2.39	-8.31
$\Delta\frac{\sigma_1}{\sigma_y}$ [‰]	+4.04	+4.33
$\Delta\frac{\sigma_2}{\sigma_y}$ [‰]	+7.67	+7.08
\dot{P}_{req}	✓	✓

that the scale of the structural performance measure makes these differences insignificant. With the structural objective normalisation, it is seen that all designs may be structurally sound. However, it is recognised that as the structural model remains to be validated, the results should therefore be used with due caution.

Table 6 presents the performance of the dual point design, for both take-off and cruise conditions. Again, these are with reference to the baseline design. As can be seen from the resulting

Table 6: Design performance (against baseline) for dual point

Parameter	Take-off	Cruise
$\Delta\eta$ [%]	+2.37	+11.0
ΔSPL [dB]	-1.42	-7.95
$\Delta\frac{\sigma_1}{\sigma_y}$ [‰]	+0.393	+0.744
$\Delta\frac{\sigma_2}{\sigma_y}$ [‰]	+7.20	+7.03
\dot{P}_{req}	✓	✓

data, gains in propulsive efficiency and reductions in noise (again at the cost of reduced structural performance), are observed. However, for the dual point design, as is expected, the gains for each operating point are not as significant for the single point designs. This further highlights the compromises required for multi-operating point designs. Nonetheless, the resulting performance still produces significant performance gains over both flight conditions. The performance of the single point and dual point cruise designs are not seen to differ too greatly and can be expected when comparing the geometries of the two resulting designs.

Considering the noise, in cruise the thickness noise dominates, and with similar designs, the noise gains are seen to be quite similar. The opposite is true for take-off where loading noise dominates. With the differing blade counts, the loading on each will be significantly different, and hence the differ-

ence in noise gains between the single point and dual point take-off designs.

In order to further illustrate design changes, Figures 13-15 show CAD representations of the resulting optimal designs.

This section has presented the performance and geometries of optimised designs for both the single and dual point objectives. It can be seen that in all cases, the routine was able to produce designs with increased performance over an arbitrary baseline design. This highlights the usefulness and potential of the optimisation routine to perform the preliminary design of a CROR blade pair.

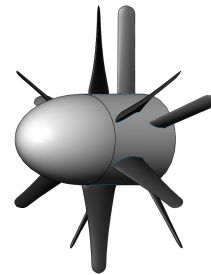


Figure 13: Cruise only design.

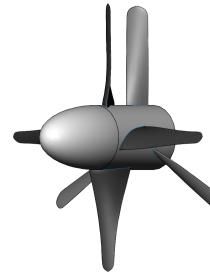


Figure 14: Take-off only design.

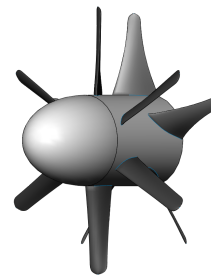


Figure 15: Simultaneous cruise and take-off design (take-off condition shown).

7. CONCLUSION

This work has presented a number of low order models for the analysis of CROR performance. Mod-

els were presented for the evaluation of aerodynamic, acoustic and structural performance. With the aerodynamic and acoustic models being validated to demonstrate their ability to capture sufficient physics to describe the CROR performance. Following this, an optimisation routine for the design of CRORs was discussed, with suitable objective functions for single point and dual point designs. Results for cruise only and take-off conditions were presented and both showed improved performance over a baseline design. Next, a design was conducted simultaneously optimising take-off and cruise performance. Again this showed improved performance over the baseline. However, performance gains for each flight phase were not as great as their single-point design counterparts.

In conclusion, it can be said that the low order models presented are suitable for preliminary analysis of CRORs. In addition to this, this work has shown the capability and potential of the optimisation routine as a preliminary design tool for CRORs. The design tool may identify a number of high performing designs which may then be further studied with higher fidelity models.

ACKNOWLEDGEMENTS

This research is supported by Mr Mike Newton, and the authors would like to extend their gratitude to him for the sponsorship of the work.

REFERENCES

- [1] Advisory Council for Aviation Research and Innovation in Europe, "Strategic Research and Innovation Agenda," Tech. Rep., 2012.
- [2] P. Busquin, P. Argüelles *et al.*, "European Aeronautics: a Vision for 2020 - Meeting Society's Needs and Winning Global Leadership." *Advisory Council for Aeronautics Research in Europe, Report*, 2001.
- [3] P. Beaumier, "A Low Order Method for Co-Axial Propeller and Rotor Performance Prediction," *29th Congress of the International Council of the Aeronautical Sciences (ICAS 2014)*, 2014.
- [4] A. Betz, "Schraubenpropeller mit geringstem Energieverlust. Mit einem Zusatz von L. Prandtl," *Nachrichten von der Gesellschaft der Wissenschaften zu Göttingen, Mathematisch-Physikalische Klasse*, vol. Bd. 3, pp. 193–217, 1919.
- [5] L. Prandtl, "Application of Hydrodynamics to Modern Aeronautics," NACA Report No. 116, Tech. Rep., 1921.
- [6] M. Abramowitz and I. A. Stegun, *Handbook of Mathematical Functions*, 10th ed., 1972.
- [7] M. De Gennaro, D. Caridi, and M. Pourkashanian, "Ffowcs Williams-Hawkings Acoustic Analogy for Simulation of Nasa SR2 Propeller Noise in Transonic Cruise Condition," *V European Conference on Computational Fluid Dynamics*, no. June, pp. 14–17, 2010.
- [8] D. Dunham, C. L. Gentry, and P. L. Coe, "Low-Speed Wind-Tunnel Tests of Single- and Counter-Rotation Propellers," *NASA TM-87656*, 1986.
- [9] D. B. Hanson, "Noise of Counter-Rotation Propellers with Non-Synchronous Rotors," *Journal of Aircraft*, vol. 22, no. 12, pp. 1097–1099, 1985.
- [10] D. B. Hanson, "Helicoidal Surface Theory for Harmonic Noise of Propellers in the Far Field," *AIAA Journal*, vol. 18, no. 10, pp. 1213–1220, 1980.
- [11] B. Magliozzi, D. B. Hanson, and R. K. Amiet, "Propeller and Propfan Noise," In *NASA Langley Research Center, Aeroacoustics of Flight Vehicles: Theory and Practice. Volume 1: Noise Sources*, 1991.
- [12] A. B. Parry, "Theoretical prediction of counter-rotating propeller noise," PhD Thesis, University of Leeds, 1988.
- [13] P. J. W. Block, "Installation Noise Measurements of Model SR and CR Propellers," *NASA Technical Memorandum 85790*, 1984.
- [14] W. Young and R. Budynas, *Roark's Formulas for Stress and Strain*, 7th ed. McGraw-Hill, 2002.
- [15] J. Yoo, "An Approximate Method of Obtaining Stress in a Propeller Blade," *Milcom 2006*, 2006.
- [16] K. E. Schoenherr, "Formulation of propeller blade strength," *Trans. Soc. Naval Architects Marine Engrs*, vol. 71, pp. 81–119, 1963.
- [17] A. J. Chipperfield, "The MATLAB Genetic Algorithm Toolbox," in *IEE Colloquium on Applied Control Techniques Using MATLAB*, 1995.
- [18] D. E. Goldberg, *Genetic Algorithms in Search, Optimization, and Machine Learning*. Reading, Massachusetts: Addison-Wesley Publishing Company, Inc., 1989.
- [19] A. Filippone, "Rapid Estimation of Airfoil Aerodynamics for Helicopter Rotors," *Journal of Aircraft*, vol. 45, no. 4, pp. 1468–1472, 2008.
- [20] B. M. Kulfan, "Universal Parametric Geometry Representation Method," *Journal of Aircraft*, vol. 45, no. 1, pp. 142–158, 2008.
- [21] T. Murata and H. Ishibuchi, "MOGA: Multi-Objective Genetic Algorithms," *Proceedings of 1995 IEEE International Conference on Evolutionary Computation*, 1995.
- [22] A. Filippone, "FLIGHT - Improving Aircraft Performance." [Online]. Available: <http://www.flight.mace.manchester.ac.uk/>